

Diffusion coefficient of a passive contaminant in a local MHD model of a turbulent accretion disc

Augusto Carballido^{1,2,*}, James M. Stone^{2,†} and James E. Pringle^{1,‡}

¹ *Institute of Astronomy, University of Cambridge, Madingley Road, Cambridge CB3 0HA, UK*

² *Department of Astrophysical Sciences, Princeton University, Princeton NJ 08544, USA*

23 September 2018

ABSTRACT

We calculate the radial diffusion coefficient for a passive contaminant in an accretion disc which is turbulent due to the action of the magnetorotational instability. Numerical MHD simulations are used to follow the evolution of a local patch of the disc using the shearing box formalism. A separate continuity equation for the mass fraction of contaminant is integrated along with the MHD system, and radial profiles of this fraction are obtained as a function of time. Solutions of a linear diffusion equation are fitted to the numerical measured profiles of the contaminant, treating the diffusion coefficient D as the fitting parameter. At early times, the value of D is found to vary, however once the contaminant is spread over scales comparable to the box size, it saturates at a steady value. The ratio of D to the transport coefficient of angular momentum due to shear stress is small. If D can be used as a proxy for the turbulent magnetic diffusivity, the effective magnetic Prandtl number $P_{\text{eff}} = \nu/D$ (where ν is the coefficient of "effective viscosity" associated with shear stress) would be large.

Key words: accretion: accretion discs – magnetohydrodynamics

1 INTRODUCTION

In order to understand the morphology and chemical composition of protoplanetary accretion discs, the radial mixing of vapour and solid material in accretion flows needs to be characterised (Morfill 1983). The distribution of dust across a turbulent disc, as a consequence of both advective and diffusive modes, will determine the mechanism which is most favourable for the assemblage of particles into planetesimals, meteoritic bodies and eventually planets. For example, there is evidence for radial upstream movement of nebular gas from the coexistence of calcium-aluminum inclusions and chondrules in meteorites (Boss 1998). Studies by Takeuchi & Lin (2002) and by Keller & Gail (2004) indicate that, for vertically isothermal *laminar* discs, there may exist an equatorial outflow capable of transporting material from the hot, inner regions to the cold, outer regions, thereby affecting the composition of bodies located in the latter zone. The material is assumed to be well coupled to the gas, which is true for particles whose size is smaller than the mean free path of the gas molecules. However, this picture may be changed if angular momentum transport in the disc is mediated by

magnetohydrodynamical turbulence driven by the magnetorotational instability (MRI) (Balbus & Hawley 1991).

The transport of a passive scalar has been used as a criterion to study diffusive processes in turbulent flows (e.g. Brandenburg, Käpylä & Mohammed 2004 and references therein). Research on the behaviour of passive tracers in turbulence has shown that there is a strong variability of dissipation and mixing rates of both scalar and velocity fields, due to small scale intermittency. It has also been shown that the central assumption of Kolmogorov scaling, that at small scales the scalar and velocity fields are isotropic in the limit of infinite Reynolds and Peclet numbers, breaks down (Warhaft 2000; Sreenivasan 1991). Although a fascinating subject, in this work we will not address many important issues that belong to the vast field of passive scalars.

Clarke & Pringle (1988) analysed the evolution of the concentration of a trace contaminant in a steady, Keplerian disc. They point out a subtlety related to the identification of a diffusion coefficient with a viscosity for turbulent accretion. Despite the fact that both are associated with velocity fluctuations in the turbulence, their effects are distinct: diffusion tends to produce a uniform mixing of material, whereas viscosity does not yield a uniform distribution of angular momentum. They found that the contaminant behaviour depends on the ratio of the diffusion coefficient to viscosity; only when this ratio is near

* E-mail: augusto@ast.cam.ac.uk

† E-mail: jstone@astro.princeton.edu

‡ E-mail: jep@ast.cam.ac.uk

or greater than unity does diffusion take place appreciably. Heyvaerts et al. (1996) have shown that in an accretion disc in which the effective viscosity is due to turbulence generated by the Balbus-Hawley instability, the associated magnetic Reynolds number is small, whereas the magnetic Prandtl number $P_m = \nu/\eta$ (where η and ν are the magnetic resistivity and the effective viscosity, respectively) is not necessarily so.

In this context, we wish to investigate the role that turbulent diffusion plays locally in the transport of a passive tracer, within a small portion of a weakly magnetised accretion disc in which the MRI operates. We use numerical MHD simulations which adopt the so-called “shearing box” model, discussed in detail by Hawley, Gammie & Balbus (1995, hereafter HGB), a useful scheme for the study of local processes in accretion flows. We extend the numerical scheme to explicitly follow the time evolution of a passive contaminant in the flow to determine the rate of turbulent mixing. We use the ideal MHD approximation to simplify the problem; this requires the magnetic field be well coupled to the gas. Although the structure of protoplanetary discs is not well known, it is likely that far from the central star, the central regions of the disc are dense and cool enough that non-ideal MHD effects such as Ohmic dissipation, ambipolar diffusion, and the Hall effect will significantly alter the MHD (Blaes & Balbus 1994; Wardle 1999; Sano et al. 2000; Stone et al. 2000; Balbus & Terquem 2001; Salmeron & Wardle 2003). Recent studies of the MRI in non-ideal MHD indicate turbulence and transport may be strongly suppressed if the magnetic Reynolds number is close to one (Hawley & Stone 1998; Sano & Miyama 1999; Fleming, Stone, & Hawley 2000; Sano & Stone 2002). It is possible that even if the MRI is suppressed in the central regions of the disc, the surface layers may be ionized by non-thermal effects and remain turbulent (Gammie 1996; Glassgold et al. 1997; Fleming & Stone 2003). Of course, by adopting the ideal MHD approximation, this study cannot be applied to regions of the disc where the ionisation fraction is so low that it is stable to the MRI: the turbulent transport of contaminants in these regions will be essentially zero. In regions where the MRI is suppressed but not eliminated, the saturation amplitude of the turbulence will be reduced, thereby reducing both the coefficient of effective viscosity ν and the turbulent coefficient D . Thus, the ratio of the two (the effective magnetic Prandtl number P_{eff}) may be independent of the level of saturation of the instability. Studying diffusion in realistic, global models of protoplanetary discs including non-ideal MHD and the vertical and radial dependence of the ionisation fraction is a challenging problem and beyond the scope of this study.

Previous work has investigated diffusive processes in different magnetohydrodynamic contexts. Yousef et al. (2003) performed forced turbulence simulations in which they obtain a value of the turbulent magnetic Prandtl number of about unity, regardless of the value of the microscopic magnetic Prandtl number. Brandenburg et al. (2004) study non-local aspects of turbulent transport by adding a second-order time derivative to the equation for the concentration of a passive contaminant, namely Fick’s law, which states the proportionality of the flux of passive scalar to the negative concentration gradient. This extra term results in a damped wave equation for the concentration. Our investi-

gation is similar, except turbulence in our models is driven by a linear instability in the background flow, rather than by an assumed forcing. Moreover, the orbital dynamics in an accretion flow strongly affect the velocity and magnetic field correlations in the turbulence, which may directly affect the turbulent diffusion.

This paper is organised as follows. In Section 2 the numerical method employed is described, including the method by which the turbulent diffusion coefficient is calculated. Results of a variety of simulations are described in Section 3, while a discussion and conclusions are presented in Section 4.

2 METHOD

2.1 Numerical Method

We use a three-dimensional version of the ZEUS code (Stone & Norman 1992a;b) in which the shearing box model of HGB is implemented. Briefly, a coordinate system is centered at a fiducial radius r_0 in a small patch of a disc, which has linear dimensions much less than r_0 . This new system corrotates at an angular velocity $\Omega_0 = \Omega(r_0)$. The x, y, z coordinates correspond to cylindrical r, φ, z coordinates, respectively. The resulting MHD equations then incorporate the effects of Coriolis forces and tidal stresses (see below). The numerical implementation of the shearing box involves boundary conditions such that the computational domain is strictly periodic in the y, z directions at all times, whereas in the x (radial) direction it is *quasiperiodic*: when a fluid element exits at one radial boundary, it reappears at the opposite radial boundary with a position and a velocity given by the shearing motion.

The passive contaminant is introduced in the code as a fraction of the gas density. In addition to the MHD equations for the shearing box,

$$\frac{\partial \rho}{\partial t} + \nabla \cdot (\rho \mathbf{v}) = 0 \quad (1)$$

$$\frac{\partial \mathbf{v}}{\partial t} + \mathbf{v} \cdot \nabla \mathbf{v} = -\frac{1}{\rho} \nabla \left(P + \frac{B^2}{8\pi} \right) + \frac{(\mathbf{B} \cdot \nabla) \mathbf{B}}{4\pi\rho} - 2\Omega \times \mathbf{v} + 3\Omega^2 x \hat{x} \quad (2)$$

$$\frac{\partial \mathbf{B}}{\partial t} = \nabla \times (\mathbf{v} \times \mathbf{B}) \quad (3)$$

$$\frac{\partial \rho \epsilon}{\partial t} + \nabla \cdot (\rho \epsilon \mathbf{v}) + P \nabla \cdot \mathbf{v} = 0 \quad (4)$$

$$P = \rho \epsilon (\gamma - 1) \quad (5)$$

where the symbols have their usual meanings, the code also solves a continuity equation for the contaminant fraction:

$$\frac{\partial f \rho}{\partial t} + \nabla \cdot (f \rho \mathbf{v}) = 0 \quad (6)$$

where f is a number between 0 and 1.

As in HGB, we use the standard values $P = P_0 = 10^{-6}$ (initial pressure), $H = 1$ (box height), and $\Omega = 10^{-3}$. Our runs adopt the same parameter values as those of model Z4 of HGB (in particular, we use a uniform strength vertical field with plasma parameter $\beta = 400$), except that we use a resolution of $88 \times 184 \times 88$ grid zones, almost three times greater in each dimension than that used in Z4. The box size is $1 \times 2\pi \times 1$.

2.2 Simulations

HGB showed that turbulence develops after a few orbits in the evolution of the shearing box (one orbit = $2\pi/\Omega$). We first run the code for 16 orbits, to ensure that turbulence has set in and is able to stir the contaminant efficiently. At $t = 16$ orbits the code is restarted and the contaminant is introduced; we set $f = 1$ for $-0.15 \leq x \leq 0.15$ and for all y and z , forming a slab inside the box. The system is then allowed to evolve for several more orbits, and the rate of radial spreading of the slab is used to determine the turbulent diffusion coefficient.

We expect statistical fluctuations in the evolution of f to be large given the chaotic nature of turbulence driven by the MRI (Winters, Balbus, & Hawley 2003). Thus, to improve our measurement we have performed 22 runs beginning at different times, reintroducing the contaminant in its original distribution each time a run is restarted, and evolving the flow for different periods. We shall group these simulations according to the length they were run, labeling each group with different letters, and each run within a group by different numbers. Run A1 was evolved for one orbit beginning at orbit 16. Runs B1 through B8 were evolved sequentially for 0.15 orbits each, starting at orbit 17 (so that run B1 provides a measurement of how the contaminant mixes in the flow during the evolution from 17.00 to 17.15 orbits; run B2 from 17.15 to 17.30 orbits, etc.). Runs C1 through C13 were evolved sequentially for 3 orbits each, starting at 18.2 orbits (so that run C1 is evolved from 18.2 to 21.2 orbits, etc.). In this way we are able to measure the turbulent mixing in the flow over 41.2 orbits of evolution.

From each run we obtain radial profiles of the azimuthally and vertically averaged contaminant fraction f at intervals of 0.05 orbits. For each one of these snapshots, we average the corresponding radial curves over the number of runs performed, and hence obtain a single curve at each time. For example, to obtain the curve that corresponds to the radial profile of f at 0.15 orbits, we can average over all 22 runs (since all were run for at least that long). However, for the curve that corresponds to the radial profile of f at 1.5 orbits, we average over the 13 runs in the group labelled C.

2.3 Calculation of diffusion coefficient

In order to calculate a value of the diffusion coefficient associated with the turbulent flow, we have chosen to solve a diffusion equation for the contaminant fraction in the radial direction with the same initial condition as that introduced in the code:

$$\frac{\partial f}{\partial t} = D \frac{\partial^2 f}{\partial x^2}, \quad (7)$$

$$f(x, 0) = \begin{cases} 1 & \text{if } |x| \leq 0.15 \\ 0 & \text{if } |x| > 0.15 \end{cases}$$

The solution of this initial value problem is

$$f(x, t) = \frac{1}{2} \left[\operatorname{erf}\left(\frac{x + 0.15}{2\sqrt{Dt}}\right) - \operatorname{erf}\left(\frac{x - 0.15}{2\sqrt{Dt}}\right) \right] \quad (8)$$

We then fit this solution to the curves obtained from the simulations, treating the diffusion coefficient D as the fitting parameter. To test whether D is constant in time,

the fitting is performed independently for each time in the evolution of the contaminant.

It is worth pointing out that we are using equation (7) as a first approximation, and it may not describe the diffusion process of the contaminant completely.

3 RESULTS

Figure 1 shows the evolution of the $f = 0.5$ isosurface of the contaminant in Run A1 at $t = 16, 16.05$ and 16.1 orbits (that is at the start of the run, and 0.05 and 0.1 orbits later). At early times, wrinkling of the surfaces on small scales is evident, as radial advective transport of the contaminant by turbulent eddies occurs. At later times, larger scale distortions appear, as the contaminant is advected on larger scales by larger eddies.

Figure 2 plots the azimuthally and vertically averaged radial profile of the contaminant from $t = 0.05$ orbits to $t = 2.75$ orbits after the contaminant is introduced. The averages are taken from all the data available at each time. Over this timescale, steady diffusion of the contaminant towards a uniform profile (consistent with the radially periodic boundary conditions) is evident.

In Figure 3 we plot fits of the model curve, equation (8), to the average radial profiles of contaminant fraction obtained from the simulations, at the same six times as shown in Figure 2. The value of the diffusion coefficient D that provides the best fit in each case is shown at the bottom of each panel. A total of 57 fits were performed, corresponding to 57 different instants in the evolution of the contaminant; Figure 3 plots six that are representative of the fitting process. The error bars shown correspond to the standard deviation of the simulation data.

The values of D obtained by fitting equation (8) every 0.05 orbits of evolution are plotted as a function of the time after the contaminant is introduced in the turbulent flow in Figure 4. During the first ~ 0.75 orbits of the evolution, D grows from approximately $1.2 \times 10^{-2} H^2/\text{orbit}$ to about $5 \times 10^{-2} H^2/\text{orbit}$. After about 0.75 orbits, D becomes more nearly constant; its value does not fall below $\approx 4 \times 10^{-2} H^2/\text{orbit}$, and does not exceed $\approx 5 \times 10^{-2} H^2/\text{orbit}$, with an average value between 1 and 3 orbits of $(4.7 \pm 1.0) \times 10^{-2} H^2/\text{orbit}$. As discussed in the next section, the change in behavior at 0.75 orbits appears to be related to the spatial extent of the contaminant, and the size of the largest turbulent eddies in the box. The diffusion time $t_{\text{diff}} \equiv H^2/D$, using the saturated value of D at late times, is 21 orbits.

It is useful to compare the magnitude of D measured from the simulations with the effective viscosity associated with shear stress, using the Prandtl number, $P_{\text{eff}} \equiv \nu/D$. The value of ν can be calculated through the relation

$$\nu = \alpha c_s H = \frac{\langle\langle w_{xy} \rangle\rangle}{P} H^2 \Omega \quad (9)$$

where c_s is the sound speed, $\langle\langle w_{xy} \rangle\rangle$ is the time- and volume-averaged value of the r - φ component of the stress tensor (magnetic plus kinetic), H is the disc scale height, and Ω is the angular frequency. The second equality follows from the fact that

$$\alpha = \frac{\langle\langle w_{xy} \rangle\rangle}{P} \quad (10)$$

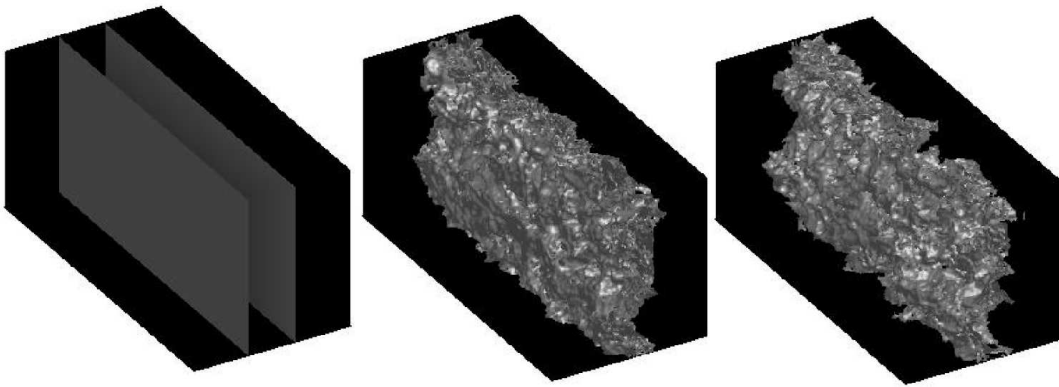


Figure 1. Evolution of the $f = 0.5$ isosurface of contaminant in Run A, starting at $t = 16$ orbits (left panel) when the contaminant is introduced into the saturated turbulence, $t = 16.05$ orbits (center panel), and $t = 16.1$ orbits (right panel).

and

$$c_s = H\Omega \quad (11)$$

Using a value for $\langle\langle w_{xy} \rangle\rangle$ which is measured directly from the simulations (including both the Reynolds and Maxwell stress), we obtain $\nu \approx 0.52H^2/\text{orbit}$. The Prandtl number is then

$$P_{\text{eff}} = \frac{\nu}{D} \quad (12)$$

$$= \frac{0.52}{0.047} \quad (13)$$

$$\approx 11 \quad (14)$$

4 DISCUSSION

Using numerical MHD simulations of turbulence driven by the MRI, we have measured the diffusion coefficient for a passive contaminant mixed by the flow. When compared to the effective viscosity associated with angular momentum transport, the diffusion coefficient is small, that is the Prandtl number $P_{\text{eff}} = \nu/D > 1$.

Of course, numerical errors are an important contribution to the diffusion rate on scales comparable to the grid spacing. However, on larger (resolved) scales up to the box size, there is strong evidence that numerical effects do not determine the diffusion rate. The only numerical errors in solving equation (6) arise in the advection step of the

ZEUS code. The magnitude and convergence rate of these errors have been studied in Stone & Norman (1992a). For the second-order van Leer scheme used in these calculations, discontinuities are diffused until they span 10-15 zones in a few dynamical times, thereafter very little numerical diffusion occurs. Figure 2 shows the profiles reach nearly uniform profiles in less than 3 orbits, indicative of a much larger diffusion rate than that associated with numerical errors revealed in the advection tests in Stone & Norman (1992a). Thus, while numerical diffusion may be important on small scales and at early times, it is unlikely to determine the evolution observed in Figure 2. Normally the effects of numerical diffusion would be assessed by repeating the simulations at different resolutions and looking for convergence. However, increasing the numerical resolution can also change the properties of the turbulence driven by the MRI on small scales; such resolution studies are less instructive in this case.

Figure 4 shows that the best fit value of the diffusion coefficient D found by fitting the analytic solution, equation (8), to the numerically computed profiles increases nearly linearly in time during the first 0.75 orbits of evolution, and thereafter saturates at a nearly constant value approximately four times the initial value. Thus, the turbulent diffusion coefficient seems to acquire a meaningful, approximately constant value only after the tracer has been spread over large scales, comparable to the box size. The possibility that the diffusion of contaminants in turbulent flows follows a non-Fickian diffusion law has been suggested pre-

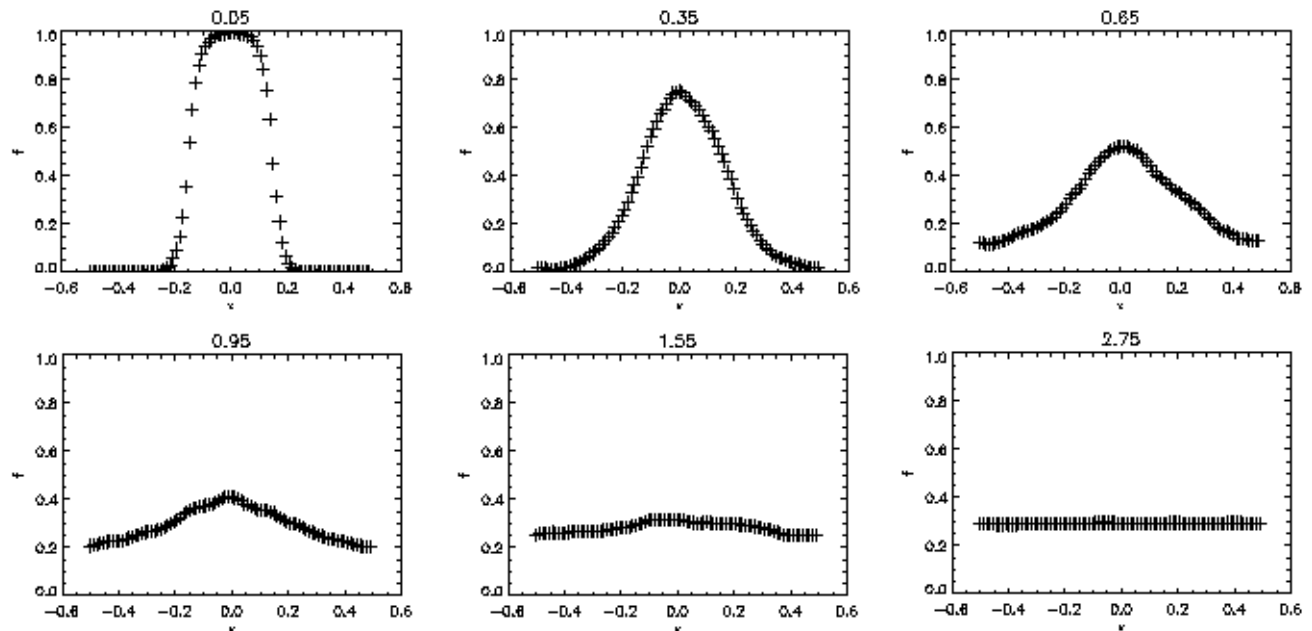


Figure 2. Evolution of the azimuthally and vertically averaged radial profile of contaminant fraction. The corresponding time after the introduction of the contaminant into the turbulent flow (in orbits) is shown above each frame. The values of f are shown at each radial grid point in the simulation.

viously by Brandenburg et al. (2004). In our case, the variation of D with time may be related to a variation in the turbulent velocity fluctuations with scale. Because turbulence driven by the MRI follows a nearly Kolmogorov scaling (HGB), the largest velocity fluctuations are on the largest scales. As the profile of the contaminant spreads, it samples larger scales, and larger amplitude eddies. Once the profile is spread across the largest scale in the simulation (the box size), no larger amplitude eddies are possible, and D becomes approximately constant. At this stage we have not performed simulations with different box sizes; the effect of changing the box size may alter the value of D , since the amplitude of the MRI turbulence is set by the box size. However, the stress would also be modified, and the overall effect would be best examined via their ratio, P_{eff} .

The fact that D varies in time for $t < 0.75$ orbits calls into question the applicability of using equation (7) to describe the evolution of the contaminant at early times. A more accurate procedure for measuring D would be to use the spatial distribution of f at $t = 0.75$ orbits as the initial condition for equation (7), and solve for the resulting evolution, so that a solution is found only for times when D is known to be constant. Although this may result in a slightly modified value for D measured from the simulations,

our primary result that $P_{\text{eff}} = \nu/D > 1$ will not change. One should also be aware of the possibility that this transport process follows anomalous diffusion (Bouchaud & Georges 1990).

If the magnetic field acted as a passive scalar in the flow, and one could associate the diffusion coefficient D with the coefficient of resistivity η , the magnetic Prandtl number would be $P_m = \nu/\eta \approx 10$, where ν is the time- and volume-averaged shear stress (Reynolds plus Maxwell) in the simulation. In studies of driven turbulence, Yousef et al. (2003) found that, for weak magnetic fields, P_m is close to unity. There are a number of reasons for this discrepancy. Firstly, the magnetic field in shearing box simulations of the MRI is clearly *not* a passive scalar, thus D may be a poor proxy for the resistivity. Perhaps just as important, the momentum transport rate in the shearing box leads to a much larger effective shear viscosity than in driven turbulence simulations, because the contributions from the Maxwell stress are larger than the Reynolds stress (HGB). Through magnetic torques, momentum transport can occur independent of mass motion that would lead to diffusion of passive contaminants.

The fact that $P_{\text{eff}} \gg 1$, so that angular momentum transport is much more efficient than diffusion of contaminants, has important consequences for the local radial

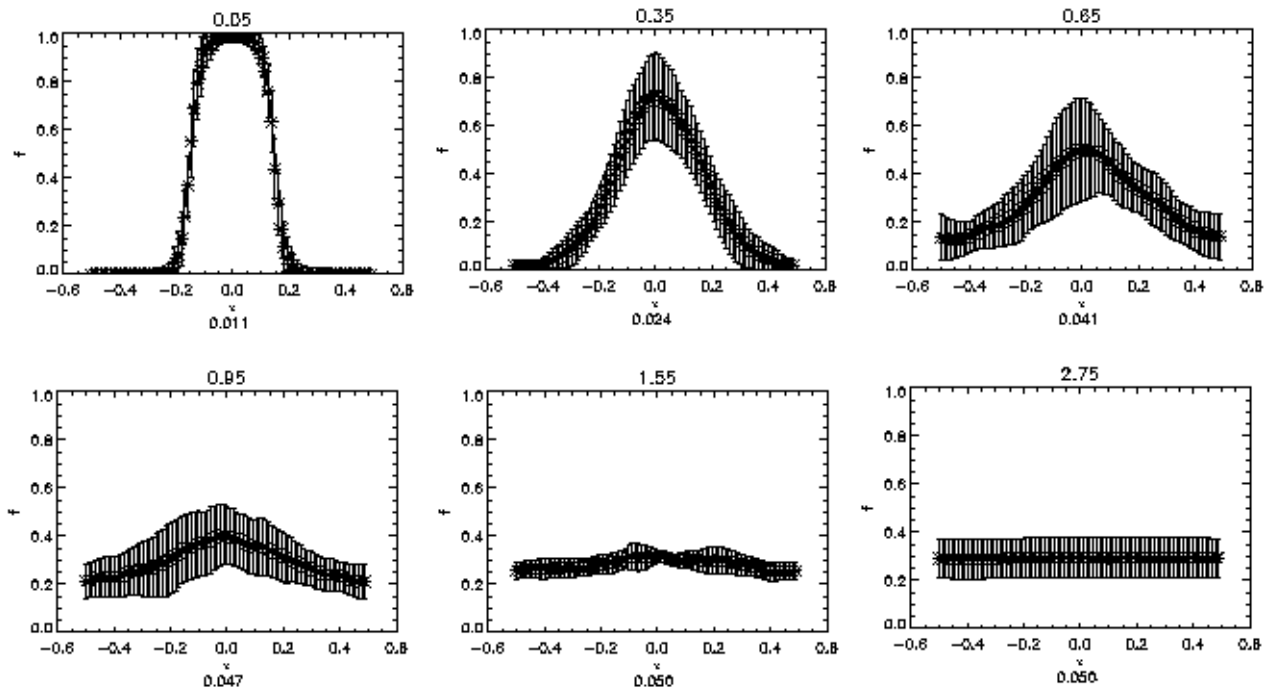


Figure 3. Fits of the theoretical curves [equation (8)] to the numerically measured average radial profiles of the contaminant shown in Figure 2. The value of the diffusion coefficient that provides the best fit is shown at the bottom of each panel, in units of H^2/orbit .

transport of small particles embedded in a magnetised disc. Global simulations will be required to determine the structure and amplitude of radial accretion flows driven by the MRI, and therefore assess whether small particles can diffuse radially outwards in the disc. One of the most important questions for global simulations of accretion discs is to determine whether large scale poloidal magnetic fields can be advected inwards by an accretion flow (leading to strong vertical fields in the inner regions of the disc), or whether they can diffuse outwards more rapidly than they are carried in (Clarke & Pringle 1988). If the diffusion coefficient D measured here were representative of the vertically averaged resistive diffusion coefficient for poloidal magnetic fields, then $P_m \gg 1$ would indicate fields would be advected inward. However, since poloidal magnetic fields drive the MRI, and since reconnection (which is an important saturation mechanism in the nonlinear regime of the MRI) can break flux-freezing, it is unlikely equation (6) can be used to describe the radial evolution of poloidal fields. Global simulations of thin Keplerian discs which can address these issues are needed.

Acknowledgements: AC acknowledges support from CONACYT scholarship 167912, thanks the Department of Astrophysical Sciences at Princeton University for their hos-

pitality, and would like to thank Gordon Ogilvie for fruitful discussions. JS is grateful for financial support from the Royal Society, the University of Cambridge, and NSF grant AST-0413788 for portions of this work.

REFERENCES

- Balbus S.A., Hawley J. F. 1991, ApJ, 376,214
 Balbus S.A., Terquem C. 2001, ApJ, 552, 235
 Blaes O.M., Balbus S.A. 1994, ApJ, 421, 163
 Boss A. 1998, Annu. Rev. Earth Planet. Sci., 26, 53
 Bouchaud J. P., Georges A. 1990, Phys. Rep., 195, 127
 Brandenburg A., Käpylä P. J., Mohammed A. 2004, Physics of Fluids, 16, 1020
 Clarke C.J., Pringle J.E. 1988, MNRAS, 235, 365
 Fleming T., Stone J.M., Hawley J.F. 2000, ApJ, 530, 464
 Fleming T., Stone J.M., 2003, ApJ, 585, 908
 Gammie C.F. 1996, ApJ, 457, 355
 Glassgold A.E., Najita J., Igea J. 1997, ApJ, 480, 344
 Hawley J. F., Gammie C. F., Balbus S. A. 1995, ApJ, 440, 742 (HGB)
 Hawley J. F., Stone J.M.. 1998, ApJ, 501, 758
 Heyvaerts J., Priest E.R., Bardou A. 1996, ApJ, 473, 403
 Keller Ch., Gail H. P. 2004, A&A, 415, 1177
 Morfill G. E. 1983, Icarus, 53, 41

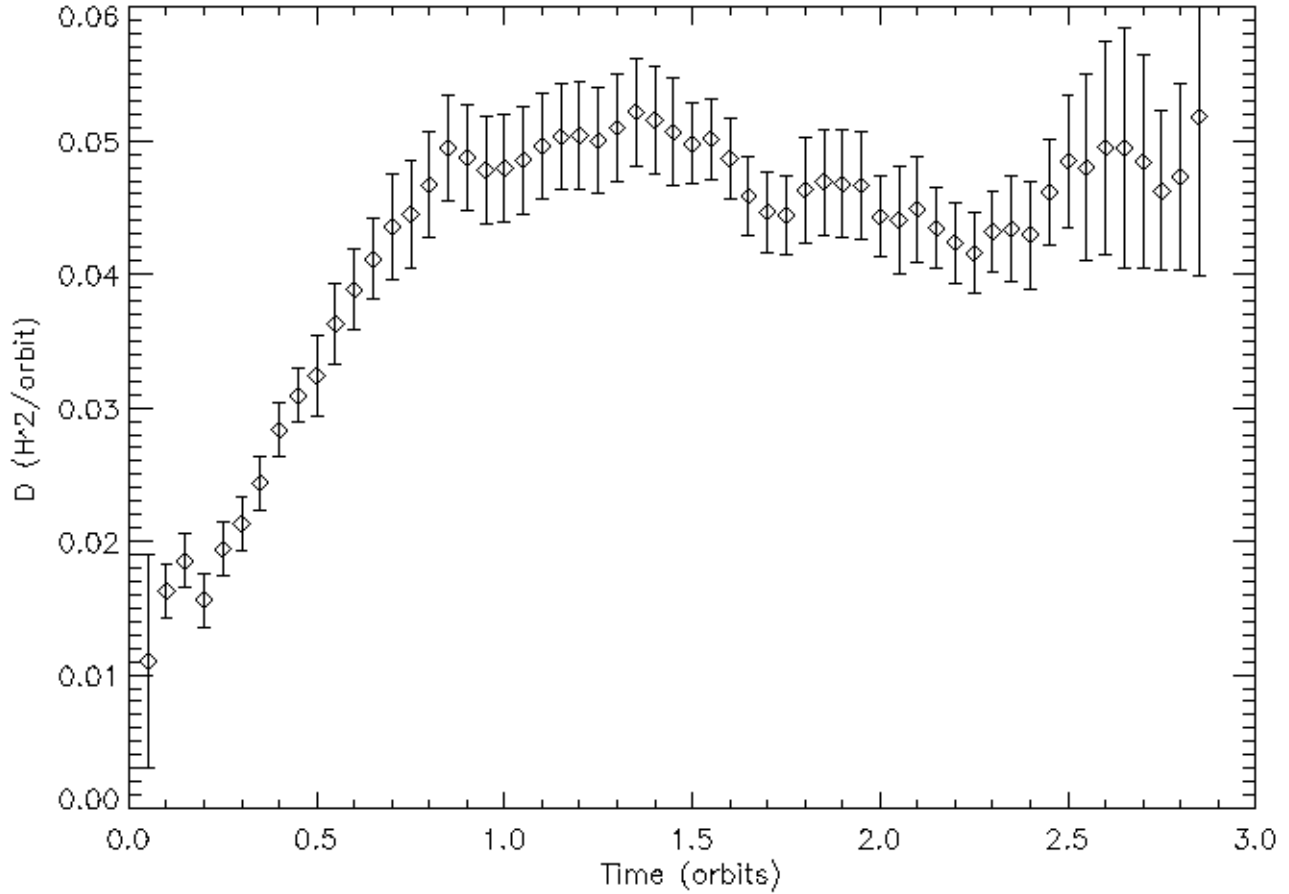


Figure 4. Turbulent diffusion coefficient D , obtained from the curve-fitting procedure described in the text, as a function of time.

Salmeron R., Wardle M., 2003, MNRAS 345, 451.
 Sano T., Miyama S.M., 1999, ApJ 515, 776
 Sano T., Miyama S.M., Umebayashi T., Nakano T., 2000, ApJ 543, 486
 Sano T., Stone J.M., 2002, ApJ, 570, 314
 Sreenivasan K. R., 1991, Proc. R. Soc. London. Ser. A 434, 165
 Stone J. M., Norman M. L. 1992a, ApJS, 80, 753
 Stone J. M., Norman M. L. 1992b, ApJS, 80, 791
 Stone J. M., Gammie C.F, Balbus S.A., Hawley J.F., 2000, Protopostars and Planets IV, ed by V. Mannings, A. Boss, & S. Russell, UA Press, Tucson, p589.
 Takeuchi T., Lin D. N. C. 2002, ApJ, 581, 1344
 Yousef T.A., Brandenburg A., Rüdiger G. 2003, A& A,411,321
 Warhaft Z., 2000, Annu. Rev. Fluid Mech., 32, 203
 Wardle M., 1999, MNRAS, 307, 849
 Winters W., Balbus S.A., Hawley J.F., 2003, MNRAS, 340, 519